GIS-Based Optimal Photovoltaic Panel Floorplanning for Residential Installations

Sara Vinco, Lorenzo Bottaccioli, Edoardo Patti, Andrea Acquaviva, Enrico Macii and Massimo Poncino
Department of Control and Computer Engineering, Politecnico di Torino, Torino, Italy
name.surname@polito.it

Abstract---**Shading is a crucial issue for the placement of PV installations, as it heavily impacts power production and the corresponding return of investment. Nonetheless, residential rooftop installations still rely on rule-of-thumb criteria and on gross estimates of the shading patterns, while more optimized approaches focus solely on the identification of suitable surfaces (e.g., roofs) in a larger geographic area (e.g., city or district). This work addresses the challenge of identifying an optimal (with respect to the overall energy production) placement of PV panels on a roof. The novel aspect of the proposed solution lies in the possibility of having a sparse, irregular placement of individual modules so as to better exploit the variance of solar data. The latter are represented in terms of the distribution of irradiance and temperature values over the roof, as elaborated from historical traces and Geographical Information System (GIS) data. Experimental results will prove the effectiveness of the algorithm through three real world case studies, and that the generated optimal solutions allow to increase power production by up to 28% with respect to rule-of-thumb solutions.**

I. Introduction

Environmental sensitivity is strongly pushing towards the replacement of energy generation based on fossil fuels with renewable energy sources. Among all kinds of renewables, photovoltaic (PV) solar energy is by far the most popular, due to decreasing costs of the devices, limited invasiveness in existing infrastructures, and economic incentives.

The placement of PV installations is clearly a critical issue; in order to maximize the return on investment, it is essential to find places with the best average solar irradiance and minimal or zero shading. Two are the categories of stakeholders that need such information, though at different granularities. On one hand, public institutions or solar energy companies require coarse-grain Geographical Information Systems (GIS) based solar data at the level of city areas or districts. On the other hand, home owners and PV suppliers/installers tend to focus on a specific surface (i.e., the rooftop) and thus need finer-grain information. While the former can afford to buy or commission such data, users usually cannot. As a result, residential rooftop installations are normally driven by rule-of-thumb criteria and by gross estimates of the shading patterns.

Some works leverage finer-grain GIS solar data to drive PV installations at a smaller scale, but in most cases they are used to identify suitable surfaces (roofs) for the installation. Only few works (e.g. [1]) use fine-grain solar data to identify the best position of PV panels on rooftops; however, they provide only qualitative feedback and do not suggest an actual placement.

In this work we specifically address the issue of the *optimal placement of a solar panel on a rooftop based on fine-grain GIS data*. In particular, given the time profile of solar irradiance and temperature, we derive a floorplanning of a solar panel consisting of N identical PV modules that optimizes the extracted power. An important novelty of the proposed approach lies in that *we allow individual modules to be placed individually*, therefore possibly yielding an unconventional, ''irregular'' floorplanning that matches the temporal distribution of solar irradiance in each point. Although this is not usually done, there is no particular technical difficulty in allowing such irregular placement.

Our method, given (i) historical irradiance and temperature data, (ii) a target area on a roof, (iii) the geometrical and electrical characteristics of the PV modules, and (iv) the desired series-parallel topology of the modules, determines a placement of N PV modules that maximizes the total extracted power, taking into account the extra overhead caused by the sparse placement. This is achieved by a heuristic algorithm that greedily maps modules to target positions on a fixed-size grid, ranked according to their suitability (mostly related to the distribution of the irradiance), and extracts the resulting total power of each configuration using the GIS data and the series-parallel overall interconnection pattern of the panel. Results show that the determined placement can extract 20-30% more energy than a traditional placement, on a yearly basis, while basically keeping the same installation cost.

II. Motivation, Background and Related Work

A. Motivation

Once the angle and the direction are determined, in absence of detailed irradiation and thermal data, rooftop panels are typically placed according to one basic rule: avoid as much as possible evident visible or possible shadings due to local obstacles (chimneys, dormers, antennas), adjacent buildings or other elements (trees, light poles, etc.). When the position is identified, the N modules of the panel are conventionally laid out by packing them together tightly. Figure 1 shows a conceptual example in which 8 modules are placed on a surface. Darker cells denote regions with higher average irradiance.

Figure 1-(a) shows the 8 modules placed using the traditional approach. Even if we exploit irradiance info, a traditional compact placement will not be able to extract the maximum possible power (e.g., modules 4, 7, and 8). Conversely, a sparse, irregular placement can better match the variance of irradiance
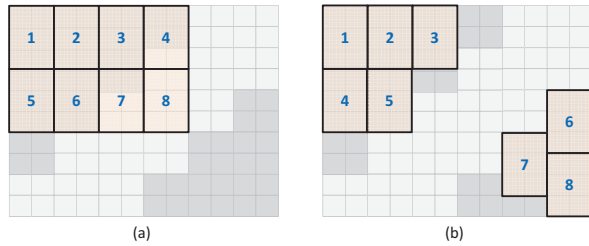
Fig. 1: A traditional PV module placement (a), and an irregular one as proposed in this work (b).
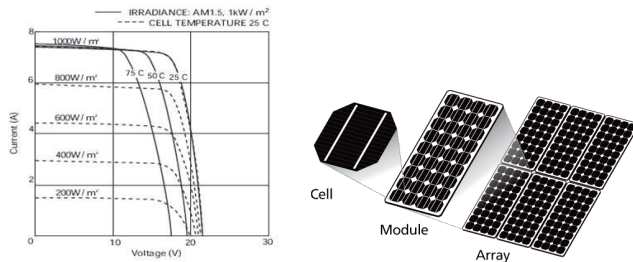

Fig. 2: I-V curve (a) and PV components hierarchy (b).

and temperature profiles and harvest a larger amount of energy. Even when the variance is small, when accrued over a long period of time, the benefit can sum up to a significant value. Figure 1-(b) shows such an example, in which the modules are placed in areas with the largest irradiance. The picture is clearly only conceptual; in practical cases the irregularity of the placement is less extreme. The irregular placement has no technical impediment with respect to a traditional one but for some wiring overhead, which we will show to be marginal.

B. Background

The basic element of a photovoltaic generator is the cell. The cell is a semiconductor diode with square, circular or rectangular shape, according to the type of cell. The electrical behaviour of a cell can be described by an ideal current source, proportional to solar irradiance, and by a diode connected in anti-parallel. A cell is described by a voltage-current (I-V) characteristic curve, which, at a given cell temperature, changes as a function of the irradiance G. When G increases, the open-circuit voltage V_{oc} increases logarithmically and the short-circuit current I_{sc} increases proportionally (dotted line in Figure 2-(a)). With fixed irradiance G, a temperature increase yields a slight increase of the short-circuit current I_{sc} which gives a decrease of the open-circuit voltage V_{oc} (solid line).

In order to increase the output power, cells are connected together according to a series/parallel organization into a PV *module*. PV modules can be further interconnected together to form a PV array, again in series or in parallel, to achieve the desired voltage and current levels. Figure 2-(b) gives a pictorial view of this hierarchy.

In PV modules, however, defects or shading can result in non-uniform irradiance in the cells involved, thus affecting the total output power. The details about how these mismatches affect the output power are described in Section III-B1. The important concept is that, because of the different power levels,

a Maximum Power Point Tracker (MPPT) needs to be used in order to maximize the efficiency. An MPPT permits the extraction of the maximum power output from the PV generator at different irradiances and temperatures.

C. Related work

Geographic Information Systems (GIS) are becoming a useful technology to model solar potential [2] and to plan the deployment of solar generators in urban environments [3]. Such GIS-based tools often start their analysis from a *Digital Surface Model* (DSM) or 3D city models obtained from LiDAR data, representing the earth surface and all objects and buildings on it. Mapwell Solar System [4] and i-Guess [5] are two GIS-based softwares for urban energy planning. Both provide information on solar radiation and PV potential; they are limited to yearly estimations only. I-SCOPE [6] is an integrated platform to give 3-D city services; it offers a solar map with yearly and monthly PV potential.

Brumen et al. [7] present a web application for PV potential assessment starting from a DSM. This tool provides data about yearly and monthly PV potential, together with information on rooftops. Schuffert et al. [8] present a methodology to derive available roof surfaces starting from LiDAR data. This methodology also estimates the yearly solar irradiance and the PV energy production in clear-sky conditions. PVWatts [9] is a GIS-based software to estimate yearly, monthly and hourly PV generation profiles using a typical meteorological year and a topographic model of $40km^2$. PVGIS [10], [11] is a web-tool that exploits solar maps to provide information on yearly and monthly PV production in Europe and Africa, e.g., sub-hourly irradiance trends in clear-sky conditions.

The presented solutions suffer from many limitations. Sub-hourly information is necessary to better estimate the optimal energy production, and low DSM resolutions (i.e., $> 1m$) do not allow to recognize obstacles on rooftops (e.g., chimneys, dormers). Moreover, to provide more accurate estimations, real weather data from weather stations [3] must be considered to compute incident radiation on rooftops in real-sky conditions. Finally, none of presented solutions provide guidelines for a smart, GIS-driven floorplanning of PV arrays.

With respect to the past literature, we propose a GIS-based methodology to determine an optimal placement of PV modules aiming at the maximization of yearly energy production, based on real-sky, sub-hourly simulations integrating high-resolution DSM with real meteorological data.

III. GIS-BASED PV FLOORPLANNING ALGORITHM

A. Problem Definition and Formulation

Our objective is to place N PV modules on a given area (not necessarily rectangular). The latter is aligned to a virtual grid whose elements are squares of side s. The sides of the area are integer multiples of s so that it consists of an integer number N_g of grid elements.

The value of s is chosen so that the panel sizes are also an integer multiple of s. Assuming that each panel is identical and has sizes $w \times h$, we have that $w = k_1 \cdot s$, $h = k_2 \cdot s$. The size of
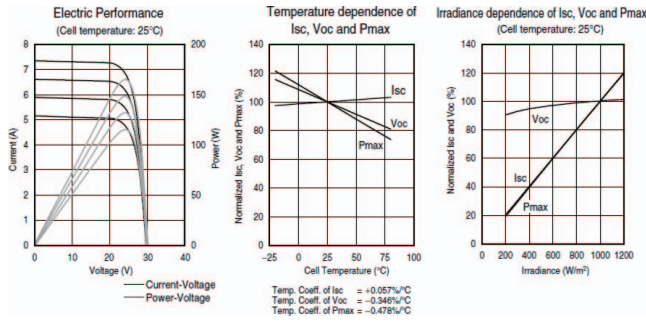
Design, Automation And Test in Europe (DATE 2018)

Fig. 3: Power characteristics of Mitsubishi's PV-MF165EB3.

the specific panel used in our analysis is 160×80cm, and we use $s = 20$cm. Notice that since grid points represent possible placement candidates, a smaller s yields more solutions, at the expense of longer computation times.

We are then given a set of measures over time of irradiance $G_i(t)$ and temperature $T_i(t)$, $i = 1, ..., N_g$. The spatial resolution of the irradiance measures determined by the solar data acquisition tool is forced to coincide with the grid granularity, so each grid point has a specific value of G and T. The process of deriving solar data with the desired granularity will be described later in Section IV.

The problem we solve in this work can be formulated as follows:

Given an available surface, a set of N_T irradiance and temperature measures for each point of a grid, and N PV modules to be placed according to a specific series-parallel topology, find the optimal placement on the surface that maximizes the energy extracted in the interval $[0, N_T]$.

B. Models

1) PV Panel Power Model: Our analysis needs a power model of an individual single PV module, because the total power extracted by the panel P_{panel} depends on its actual series/parallel topology and is in general different from the sum of the power of the individual modules.

Given a $m \times n$ series-parallel interconnection (i.e., n parallel strings each of m modules in series), the total power is obtained as $P_{panel} = V_{panel} \cdot I_{panel}$, where:

$$\begin{cases} V_{panel} &= \min_{j=1,...,n}(\sum_{i=1,...,m} V_{module,ij}) \\ I_{panel} &= \sum_{j=1,...,n}(\min_{i=1,...,m} I_{module,ij}) \end{cases}$$

and $V_{module,ij}$ and $I_{module,ij}$ are the voltage and current extracted from the i-th module in the j-th string.

In our setup, we consider a PV-MF165EB3 module by Mitsubishi, for which we derived an empirical model of V_{module} and I_{module} as a function of irradiance G and temperature T from information available in the datasheet (Figure 3). We assume that each module extracts the maximum power, i.e., V_{module} and I_{module} are the maximum power voltage and current, and $P_{module} \equiv P_{max}$.

The model derivation is done as follows:

1) Using the rightmost plot of Figure 3 we first derive the equations expressing the dependence of V_{oc}, I_{sc}

and P_{max} (i.e., P_{module} in our terminology) with respect to irradiance G. These plots are normalized with respect to reference values (at 25^oC temperature and $G = 1000W/cm^2$) of $V_{oc,ref} = 30.4V$, $I_{sc,ref} = 7.36A$, and $P_{max,ref} = 165W$, as reported in the datasheet.

2) Using the middle plot, we replace $V_{oc,ref}$, $I_{sc,ref}$, and $P_{max,ref}$ with functions that express their dependence on temperature, yielding equations for V_{oc}, I_{sc}, and P_{max} that include the dependence on G and T.

3) The above analysis does not consider the important fact that T and G are obviously correlated: when irradiance is high, temperature will also be high. We therefore correct ambient temperature T with a term depending on G, according to the model of [12]. The actual module temperature T_{act} is modeled as $T + k \cdot G$, where $k = \frac{\alpha}{h_c}$ is the ratio of the absorptivity of the roof divided by a convective and radiative loss factor ($15 \frac{WK}{m^2}$) [13].

4) The last step is to derive V_{module} and I_{module} from V_{oc} and I_{sc}. To this purpose, we exploit the fact that the maximum power voltage of the module is roughly independent of the irradiance and is $\approx 80\%$ (24V) of V_{oc} (leftmost plot of Figure 3). This allows to express V_{module} as a function of G and T. Since the relation between I_{module} and I_{sc} is more complex to extract, we simply derive it as the ratio of P_{max} and V_{module}.

These processes result into the following equations:

$$\begin{aligned} T_{act} &= T + k \cdot G \\ P_{module}(G,T) &= 165 \cdot (1.12 - 0.048 T_{act}) \cdot 10^{-3} G \\ V_{module}(G,T) &= 24 \cdot (1.08 - 0.34 T_{act}) \cdot (0.875 + 0.000125G) \\ I_{module}(G,T) &= P_{module}(G,T)/V_{module}(G,T) \end{aligned}$$

2) Wiring Overhead Characterization: The use of a loose placement of the PV modules incurs in an obvious wiring overhead, causing power loss and cost increase. In this work, we only consider the power overhead.
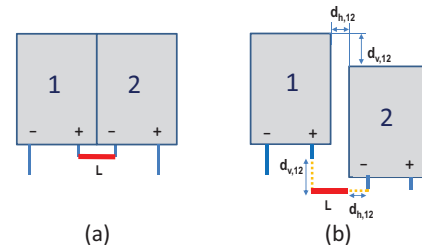

Fig. 4: Wiring overhead characterization.

Figure 4 exemplifies the problem for the series connection of two modules (1 and 2). Even in a compact placement (Figure 4-(a)), some wiring is needed (the thick red connection) between the corresponding terminals. When we distance them vertically by $d_v^{1,2}$ and horizontally by $d_h^{1,2}$ (Figure 4-(b)), the extra wiring is simply given by the sum of the two displacements (the dotted orange lines), since we have to subtract the length L of the default connector. Notice that in a real scenario we actually have shorter connections, since we are not forced to route wires along the (x,y) directions.

For the generic serial interconnection of N_s modules, the overhead will simply by given by: $L_{ovh} = \sum_{i=1}^{N_s-1} (d_v^{i,i+1} + d_h^{i,i+1})$. Knowing the current and the unit resistance of the wire used for the connection, we can compute the power drop incurred by the extra cable (RI^2).

For the parallel connection of the strings, conversely, the overhead can be neglected. In fact, typical PV installations with two or more strings do not wire the serial strings ''manually'', but do it through a *combiner box* [14], which would be used anyway even for the traditional floorplanning.

C. Floorplanning Algorithm

The calculation of the optimal placement requires an exhaustive enumeration of all possible candidate grid points, which becomes quickly unfeasible even for small areas. The solution space has a worst case size of $O(N_g^N)$; assuming to place $N = 20$ modules on a 100 m^2 surface, a grid of 20 cm implies $N_g = 2500$ candidates points, yielding a space of $O(10^{67})$ solutions. Notice that it is not possible to introduce bounds on the enumeration because the total extracted power can be computed only when all the modules are placed, because it is not possible to sum the power of the individual modules. For this reason, we devised a simple and efficient greedy approximation to the solution based on a ranking of a ''suitability'' metric for all the grid points. Given this metric, the algorithm simply allocates modules greedily, by selecting candidate points in decreasing order of suitability.

The suitability metric should distill the temporal traces into a compact signature that synthesizes the distribution of G and T values. The obvious choice of using the average is not a good choice because the typical distributions of irradiance and temperature are strongly skewed towards smaller values, and the average is not a representative value.

As a more aggregate indicator, we rather use the k-th *percentile of the distribution* as a compact metric, which represents the value below which $k\%$ of the samples fall. Specifically, we choose the 75-th percentile. Larger values of the percentile identify distributions that are more skewed towards the upper range of the values; therefore, the suitability metric should combine the percentiles of G (favoring larger values since larger G values are beneficial) and T (favoring smaller values, since smaller T values are beneficial).

However, mixing two percentiles should be done carefully and with the appropriate weight. From Figure 3, we see that G affects the output power way more than temperature: over a range of $[200 - 1000]W/cm^2$, the power changes by 5x, whereas typical T ranges only change power by $\pm20\%$ at most. Therefore, the suitability metric uses only the 75-percentile of G, and temperature is used as a corrective factor $f(T)$ that tracks the dP_{max}/dT of the middle plot of Figure 3. The suitability s_{ij} in each grid point (i,j) is thus obtained as $s_{ij} = p_{75}^{G_{ij}} \cdot f(T)$, where $p_{75}^{G_{ij}}$ is the 75-th percentile of G in the position (i,j).

Figure 5 shows a pseudo-code of the algorithm.

As in any greedy algorithm, the steps are relatively straightforward. First (Line 1) the suitability matrix $\mathbf{S}$ is computed as

Inputs:
- **W·H**: width and height of the panel placement area
- **N$_g$**: number of valid grid elements (≤ **W·H**)
- **N**: # of identical PV modules to be placed
- **m,n**: series (**m**) /parallel (**n**) topology of the panel (**m·n = N**)
- **G[i,j,t]**, **T$_i$[i,j,t]**: Irradiance and temperature matrices for each grid point **i,=1,...,W, j=1,...,H,** and for each time instant **t ∈ [1,N$_T$]**
- **V$_{module}$(G,T)**, **I$_{module}$(G,T)**: model of PV module voltage and current as a function of G and T   (section III.C)

Output:
- **P**: array of **N** grid coordinates representing the placement of the i-th module

Algorithm:
```
1.    Calculate the suitability matrix S[i,j] for each grid position (i,j)
      from G and T (75-th percentile of G with T correction factor)
2.    L = array of grid positions (x,y) sorted grid in non-increasing
      order of suitability (wiring overhead is used as a tie-breaker)
3.    j=1
4.    for each module i=1,..., N
5.        if L[j] < distance threshold
6.            P[i] ← L[j]
7.            remove from L grid points covered by current assignment
8.        endif
9.        j ← j+1
10.   endfor
11.   return P
```

Fig. 5: Algorithms inputs and pseudo-code.

described above. In Line 2, we calculate an array $\mathbf{L}$ of grid coordinates, sorted in decreasing order of their value of $\mathbf{S}$. In case of identical values of suitability, the distance from the already placed modules is used as a tie-breaker (closer grid points have higher rank). We then iterate (Line 4) over the N modules, in series-first order, i.e., modules belonging to a series string are enumerated before moving to another string. In Line 5 we introduce an important filter on the solutions. Although the wiring overhead is already counted in the sorting, it is just a tie-breaker. It might occasionally be the case that a given $L[j]$ has a high suitability but is quite far apart from the already placed modules. To this purpose we consider only coordinates $L[j]$ that do not exceed a given *distance threshold*; the latter is empirically determined as twice the average distance of the already placed modules.

The i-th module is then placed in the j-th position according to the previously computed ranking (Line 6). Since a module occupies more $k_1 \cdot k_2$ grid points (see Section III.A), all these ''covered'' points are clearly unusable and must therefore be removed from $\mathbf{L}$ (Line 7). The algorithm marks as unusable also any grid coordinate that is not surrounded anymore by enough free grid cells to host a panel.

We then pick (Line 9) the next coordinate from $\mathbf{L}$ after the removal of covered points. The loop terminates when the N panels have been placed.

IV. SOLAR DATA EXTRACTION

The proposed PV floorplanning algorithm builds upon the assumption that fine-grain distributions of irradiance and temperature are available for a roof with a fine grain granularity over a significant period of time. This work adopts the software infrastructure built in [15] as enabling technology, to derive the necessary inputs by relying on GIS data.

Input GIS data are mainly expressed through a DSM a high-resolution raster image representing terrain elevation of buildings of interest. The DSM allows to recognize encumbrances over the roof (e.g. chimneys and dormers), that prevent the deployment of PV panels, and to estimate the evolution of shadows over the roof over one year, with 15 minutes intervals. The result is the *identification of the suitable area*, i.e., of the area of the roof that can be used for the placement of PV panels. The area is then aligned to the virtual grid to obtain the inputs for the placement algorithm, i.e., the dimension of the area (parameters W and H) and the valid grid elements (N_g).

The evolution of temperature and irradiance over time is obtained by combining weather data, retrieved from personal or third-party weather stations [16], with the shadow model. Solar radiation is decomposed to estimate the incident global radiation, by additionally considering the attenuation caused by air pollution (i.e., *Linke turbidity coefficient* [11]). Solar radiation decomposition requires as inputs both the direct normal incident radiation and the diffuse horizontal incident radiation [17]. If the weather station only provides global horizontal radiation, incident radiation is derived through state-of-the-art decomposition models [18].

V. EXPERIMENTAL RESULTS

A. Experimental Setup

We applied the algorithm on roofs of three industrial buildings, shown in Figure 6-(a). They are lean-to roofs of approximately 49m×12m, facing S/S-W with inclination of 26°. The colored areas of Figure 6-(a) highlight the identified suitable areas. The figure highlights that some parts of the roofs are discarded, due to the presence of encumbrances - this is especially evident for roof 1, where pipes occupy a large space. The suitable area is then aligned to the 20cm grid. The key feature of the roofs are reported in Table I.
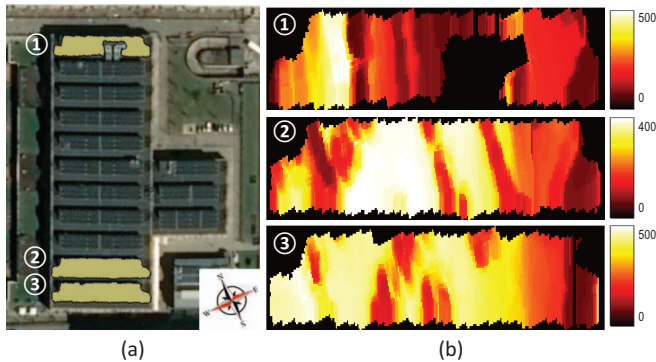

Fig. 6: Roofs used for the experimental analysis (a), and corresponding irradiance distributions (b).

The solar data extraction flow described in Section IV has then been used to derive the evolution of irradiance and temperature over time for the roofs. Despite of the geographical proximity, the roofs have quite different irradiance distributions. Figure 6-(b) shows the 75th percentile of irradiance distribution (brighter

TABLE I: Characteristics of each roof, and power production of the proposed PV floorplanning algorithm with respect to traditional placements.

| Roof | WxL | N_g | N | PV system production | | |
| | | | | Traditional | Proposed algorithm | |
				MWh	MWh	%
Roof 1	287x51	9,416	16	3.430	4.094	+19.37
			32	6.729	7.499	+11.44
Roof 2	298x51	11,892	16	2.971	3.619	+21.85
			32	5.941	7.404	+23.63
Roof 3	298x52	11,672	16	2.957	3.642	+23.16
			32	5.746	7.405	+28.86

colors represent a larger irradiation). All roofs tend to have the least irradiated grid elements on their right-hand side, as an effect of roof orientation. In general, irradiance is quite non-uniform, and the variance is quite heterogeneous over the different roofs; this is especially evident for Roof 1, as the pipes tend to lower irradiance over a wide area of the roof. Notice that this map does not include the effect of temperature.

B. Simulation Results

We run the PV floorplanning algorithm twice on the three roofs to place $N = 16$ and $N = 32$ panels. The panels are always organized with series of 8 panels ($m = 8$). The execution time of the placement algorithm is proportional to the number of valid grid elements and to the number of panels to be placed, and required less than 120s under all configurations on an Intel 8-core i7 server with 15.4GB of RAM. Due to the large number of grid elements (almost 12,000 for roofs 2 and 3), it is not possible to compare our results against an exhaustive algorithm.

Figure 7 compares the loose placements generated by our algorithm against traditional "compact" placements. Colored rectangles represent panels, with panels of the same color belonging to the same series string. Due to space constraints, the figure reports only the experiments run for $N = 32$.

The compact placements (a-c) are placed in the most irradiated area of the roof; notice that these placements are determined using accurate spatio-temporal irradiance information that are not normally available to installers. Therefore, we are comparing our solution to a particularly "good" reference.

The placements resulting from our floorplanning algorithm are shown in Figure 7-(d-f). They clearly tend to be placed nearby the traditional placements (e.g., compare (a) and (d)), yet the are sparser, since they try to exploit fine-grain differences in the distribution of irradiance and temperature. This is clearly visible for example in the triangular shape of the placement in (e), that matches the irradiance variation in that region of Roof 2 (Figure 6-(b)).

Table I clearly shows that our PV floorplanning can significantly improve the energy production on a yearly basis, with improvements that range from 11% to 28%. Obviously, the magnitude of the benefit is proportional to the available space; this explains the smaller improvements for Roof 1, which has fewer valid grid points than the other roofs.

We can also notice how more irradiated roofs improve the benefit of a customized placement; Roof 1 has a sensibly
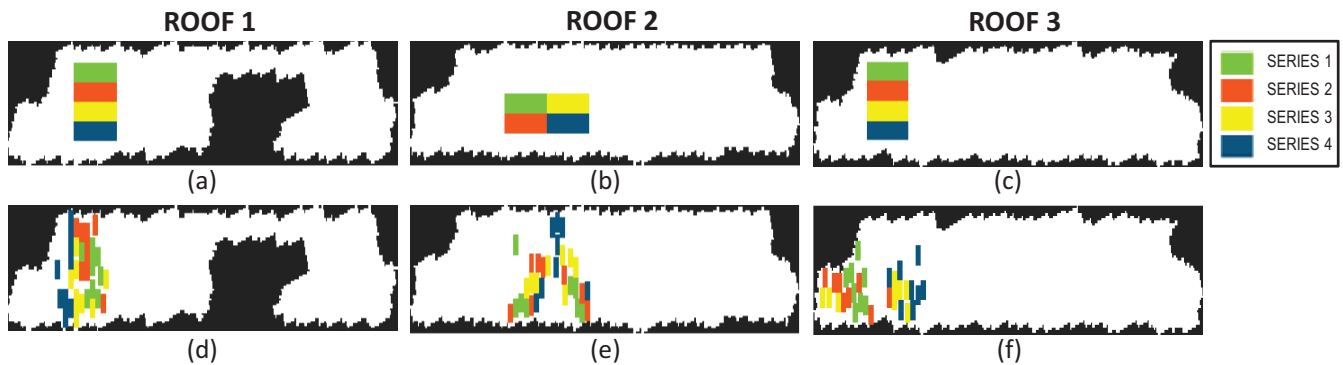
Fig. 7: Traditional PV panel placements (a-c) and placements resulting from the PV floorplanning algorithm (d-f). Colored rectangles represent panel positions, and panels of the same color are connected in series.

smaller benefit from the placement than the other two, as a result of a clearly visible lower average irradiance (Figure 6-(b)).

The sensible improvements obtained by our placement, however, are not just due to a positioning of modules that matches irradiance and temperature. Our placement is also *topology-aware*; by enumerating modules in series-first fashion, it guarantees that the bottleneck effect in a series string due to a ''weak'' module (which determines the current of the entire string) cannot occur. This effect is visible in Roof 1: the traditional and modified placements occupy more or less the same portion of the roof, and therefore they are subject to similar G and T conditions; however, the energy extracted in the placements differ by 11.4%, as mostly due to avoiding the ''weak'' module issue.

C. Overhead Assessment

For the calculation of the wiring overhead, we assume the use of an AWG 10 cable with resistive loss of $\approx 7m\Omega/m$, and an approximate cost of $1\$/m$. As a conservative calculation of the overhead, we assume a 4A current in a series string (corresponding to an irradiance of $600W/cm^2$). The power would be $RI^2 \approx 0.11W/m$ for each meter of extra cable in the string, i.e., $\approx 0.5kW/m$ of energy in one year (assuming 50% of the time at zero current for dark periods). If we multiply this number for 8 strings, and compare it to the figures of Table I, the overhead is approximately only $0.05\%/m$. Our wiring overhead is in the order of 20 meters for the worst-case solutions, so both power and cost overheads are not an issue. The placement algorithm does not directly include power overhead, if not indirectly by restricting the greedy choices as described in Section III.

VI. CONCLUSIONS

In this work we showed how, by relaxing the constraint of compactness, and by exploiting fine-grain spatio-temporal irradiance and temperature information, it is possible to determine a placement of a set of PV modules that sensibly increases the extracted energy of a PV installation, roughly at iso-cost. Our method relies on (i) an accurate GIS-based solar data extraction framework, and (ii) simple models and algorithms to determine the placement.

We demonstrated the application of the method to three real industrial roofs, showing an energy production increase as much as 28% larger than a traditional PV installation.

REFERENCES

[1] T. Voegtle, E. Steinle, and D. Tovari, ''Airborne laserscanning data for determination of suitable areas for photovoltaics,'' *ISPRS LS*, 2005.

[2] S. Freitas, C. Catita, P. Redweik, and M. Brito, ''Modelling solar potential in the urban environment: State-of-the-art review,'' *Renew. Sustainable Energy Rev.*, vol. 41, pp. 915--931, 2015.

[3] B. Resch, G. Sagl, T. Törnros, A. Bachmaier, J.-B. Eggers, S. Herkel, S. Narmsara, and H. Gündra, ''GIS-based planning and modeling for renewable energy: Challenges and future research avenues,'' *ISPRS IJGI*, vol. 3, no. 2, pp. 662--692, 2014.

[4] Mapdwell Solar System. http://www.mapdwell.com.

[5] L. de Sousa, C. Eykamp, U. Leopold, O. Baume, and C. Braun, ''iguess-a web based system integrating urban energy planning and assessment modelling for multi-scale spatial decision making,'' in *iEMSs 2012*, 2012.

[6] R. De Amicis, G. Conti, D. Patti, M. Ford, and P. Elisei, ''I-scope-interoperable smart city services through an open platform for urban ecosystems,'' 2012, http://www.iscopeproject.net.

[7] M. Brumenm, N. Lukac, and B. Zalik, ''GIS application for solar potential estimation on buildings roofs,'' in *IARIA WEB*, 2015.

[8] S. Schuffert, ''An automatic data driven approach to derive photovoltaic-suitable roof surfaces from als data,'' in *IEEE JURSE*, 2013, pp. 267--270.

[9] B. Marion and M. Anderberg, ''PVWATTS - an online performance calculator for grid-connected PV systems,'' in *ASES SOLAR*, 2000, pp. 119--124.

[10] M. Suri, T. Huld, E. Dunlop, and T. Cebecauer, ''Geographic aspects of photovoltaics in europe: contribution of the pvgis website,'' *IEEE J-STARS*, vol. 1, no. 1, pp. 34--41, 2008.

[11] PVGIS. Performance of grid-connected PV. http://re.jrc.ec.europa.eu/pvgis/apps4/pvest.php.

[12] F. Brihmat and S. Mekhtoub, ''PV cell temperature/PV power output relationships homer methodology calculation,'' in *IJSER*, vol. 1, no. 02. International Publisher &C. O, 2014.

[13] J. A. Jakubiec and C. F. Reinhart, ''A method for predicting city-wide electricity gains from photovoltaic panels based on lidar and gis data combined with hourly daysim simulations,'' *Solar Energy*, vol. 93, pp. 127--143, 2013.

[14] S. P. World, ''What is a combiner box?'' https://www.solarpowerworldonline.com.

[15] L. Bottaccioli, E. Patti, E. Macii, and A. Acquaviva, ''GIS-based software infrastructure to model PV generation in fine-grained spatio-temporal domain,'' *IEEE Systems Journal*, 2017.

[16] Weather Underground. http://www.wunderground.com.

[17] M. Šúri and J. Hofierka, ''A new gis-based solar radiation model and its application to photovoltaic assessments,'' *Trans. on GIS*, vol. 8, no. 2, pp. 175--190, 2004.

[18] N. Engerer, ''Minute resolution estimates of the diffuse fraction of global irradiance for southeastern australia,'' *Solar Energy*, vol. 116, pp. 215--237, 2015.